PAPER

Check for updates

Preparation and properties of bio-based degradable polybenzoxazines containing dihydrazone-based dynamic bonds†

Aying Wang,[a] Yifen Xu,[b] Wenli Zhao,[a] Jinning Zhang,[a] Fengjun Chen,[a] Zhongxiang Xia,[a] Lidong Zhang,[a] Jing Song,[a] Lixian Yin*[c] and Zhi Wang (ID) *[a]

Benzoxazine resins are widely used in the aerospace and electronics industries due to their high thermal stability and mechanical performance. However, their reliance on petroleum-based precursors and permanent crosslinked networks hinders recyclability, thereby creating environmental challenges. Although existing methods to introduce degradable bonds can improve recyclability, they often compromise thermal performance. To address these issues, we adopted a "rigid conjugated dynamic dihydrazone bond + bio-based synergy" strategy and designed a bio-based benzoxazine resin by synthesizing dihydrazone-containing bisphenol monomers from bio-vanillin and hydrazine hydrate, followed by polymerization with furfurylamine. This strategy incorporated acid-labile dynamic bonds into the crosslinked network while preserving thermal stability. The resin exhibited a char yield of 59.5% at 800 °C, comparable to those of petroleum-based analogues. Moreover, the dynamic network enabled controlled degradation under three conditions: elevated temperature, acetone–water mixtures (2 : 8, v/v), and 0.1 M HCl at 50 °C. In carbon fiber composites, 96% of the original fiber strength (2.64 *vs.* 2.75 GPa) was retained after 24 hours of resin decomposition, with minimal surface damage. This work demonstrates a bio-based approach for balancing thermal performance and recyclability in thermosetting composites, providing a practical pathway toward sustainable high-performance materials.

1. Introduction

Benzoxazine compounds, recognized as a novel class of polymer materials, are renowned for their excellent flame retardancy and thermal stability, and significant progress has been made in this area in recent years.[1–3] Beyond these properties, benzoxazine resins exhibit a comprehensive array of additional advantages, including near-zero shrinkage during curing, exceptional molecular design flexibility, and a by-product-free curing process that releases no small molecules.[3,4] Synthesis of benzoxazines is typically accomplished *via* the Mannich reaction, a versatile process utilizing diverse combinations of phenolic compounds, amines, and aldehydes. This reaction's versatility facilitates the design of benzoxazine monomers with tailored properties through reactant variation. When heated, with or without catalysts, benzoxazines undergo ring-opening polymerization, forming a three-dimensional network structure characteristic of polybenzoxazines.[5] However, their raw materials remain predominantly derived from petrochemical sources.[6] Given the rapid depletion of fossil fuels and petroleum reserves, coupled with the increasingly severe greenhouse effect, bio-based polymers are growing in prominence from the perspectives of environmental protection and sustainable development.[7] Producing bio-derived polymer materials utilizing renewable resources represents an approach capable of significantly reducing environmental pollution. Consequently, driven by carbon-neutrality strategies, the development of benzoxazine resins that combine high performance with environmental friendliness has become a major research focus in the polymer field. Although traditional petroleum-derived systems exhibit excellent thermal stability and mechanical strength, their non-renewable nature and environmental burden conflict with sustainable development goals. Novel bio-based benzoxazines, designed synergistically from renewable raw materials (such as lignin,[8,9] cardanol,[10,11] vanillin,[12,13] eugenol,[14] guaiacol,[15–17] vegetable oils,[18,19] and curcumin[20–22]) and bio-amines (*e.g.*,

[a] School of Materials Science and Engineering, North University of China, Taiyuan, Shanxi, 030051, China. E-mail: shikouri@163.com

[b] Aerospace Research Institute of Materials & Processing Technology, Beijing, 100076, China

[c] College of Mechatronic Engineering, North University of China, Taiyuan, Shanxi, 030051, China. E-mail: yinlixian@nuc.edu.cn

furfurylamine,[23–27] stearylamine[15,28] and dehydrodiamine[29]), have achieved low carbon emissions and cost-effectiveness.[3] Supporting this, Yuan *et al.*[30] synthesized an innovative bis-benzoxazine derivative from vanillin and furfurylamine *via* the Mannich reaction, exhibiting a char yield of >60.0% at 800 °C. Similarly, Liu *et al.*[24] developed two trifunctional monomers using biomass-derived diphenolic acid, tyramine, tyrosol, and furfurylamine in green solvents (ethanol/water), achieving remarkably low melting points (61 °C and 49 °C) and char yields of >55.0% at 800 °C. Sheng *et al.*[31] likewise prepared bio-based bis-benzoxazines from novel biodiamines and sesamol, achieving char yields of >60.0% at 800 °C. Nevertheless, these systems continue to confront the challenge of persistent waste buildup due to their inherent non-degradability.[32–34]

To break through the degradation challenge, researchers have reconstructed crosslinked networks by introducing dynamic covalent bonds including ester bonds,[35–37] disulfide bonds,[38,39] Schiff base bonds,[40,41] and boronic ester bonds.[42,43] Within polymer networks, these dynamic covalent bonds exhibit exceptional integrated properties due to their capability of reversible cleavage and reformation under specific environmental stimuli such as temperature changes, pH variations, and light exposure. This unique structural characteristic and their associated performance attributes make them a focal point of research for developing reusable thermoset polymer materials. Representative cases reveal performance trade-offs: Antoine Adjaoud's[44] team developed isosorbide-based polybenzoxazines with ester bonds (char yield: <47.5% and 5-day degradation). Similarly, Xuan Zhou *et al.*[45] reported vanillin-derived benzoxazine-epoxy resins (P-AE-MV) containing dynamic imine bonds (char yield: 11.9% and 30-minute degradation). Furthermore, Qu *et al.*[46] fabricated a bio-based reprocessable polybenzoxazine vitrimer incorporating dynamic imine bonds, demonstrating degradation within 29 minutes in an acidic THF/water solution at 50 °C, while exhibiting a char residue of 19.27% at 800 °C. Although these systems confer degradability, their thermal stability (char yield typically <50%) is insufficient to meet the demands of aerospace and other fields.

To resolve this persistent imbalance between thermal stability and degradability, incorporating rigid conjugated dynamic bonds, such as spirocyclic acetal linkages or dihydrazone units, has emerged as a promising strategy. Demonstrating this approach, Prashansa Gupta *et al.*[47] reported polybenzoxazine thermosets featuring intrinsically cross-linked rigid spirocyclic acetal bonds within the monomer. While these materials exhibited high char yields (>50%, up to 62%) at 800 °C, they remained incapable of complete degradation. However, Xu *et al.*[48] employed lignin-derived vanillin and hydrazine hydrate to synthesize a dihydrazone-containing epoxy monomer through condensation and epichlorohydrin reactions. Crosslinking this monomer yielded a novel dihydrazone-based covalent adaptable network (CAN), which demonstrated both excellent thermal stability and full dissolution within 2 hours in a 0.1 M HCl/acetone/water (8 : 2, v/v) solution at 50 °C.

Consequently, dihydrazone bonds featuring rigid π-conjugated bis-Schiff base structures are strongly positioned to resolve the stability–degradability imbalance.

Herein, a "rigid conjugated dynamic dihydrazone bond + bio-based synergy" strategy is adopted to synthesize a novel bio-based benzoxazine resin that synergizes high thermal resistance and degradability. In terms of raw material design, two bio-based precursors are selected: furfurylamine (derived from cellulose-derived furfural,[49] a bio-based chemical certified by the US Department of Energy[50]) participates in the crosslinking network through its furan ring, enhancing the density of the crosslinking network and thermal stability;[51] vanillin, as a renewable phenolic source, is modified with hydrazine hydrate at the *para*-formyl group to form a bisphenol structure containing a rigid conjugated dynamic dihydrazone bond,[48] enabling dynamic degradation. This achieves synergistic optimization of material properties; the cured resin exhibits degradation behavior regulated by temperature, acidity, and solvent type, with a char yield over 50%, significantly superior to existing dynamic bond systems of bio-based benzoxazines (residual carbon content of 11.9%–47.5%). Meanwhile, the furan ring's hydrogen-bonding interactions and the rigid conjugated structure ensure exceptional heat resistance and flame retardancy (validated by thermogravimetric analysis and microcombustion calorimetry). At the application level, the carbon fiber composites prepared from this resin maintain the chemical structure and morphology of the fibers intact during recycling, while the degradation products are derived from bio-based components, ensuring environmental compatibility. This study pioneers the integration of dynamic dihydrazone bonds into bio-based benzoxazines through molecular design, achieving a high char yield (>50%) alongside rapid degradation. All raw materials except paraformaldehyde are bio-derived, establishing a groundbreaking "structure–performance–sustainability" paradigm for green high-performance resin development.

2. Experimental section

2.1. Materials

Paraformaldehyde (97%) was purchased from Shanghai Tenghuai Biotechnology Co. Vanillin (99.0%), hydrated hydrazine (AR 80%), furfurylamine (99%) and bisphenol A (>99%) were purchased from Shanghai Aladdin Biochemical Technology Co. Acetone (AR), anhydrous ethanol (AR), *N,N*-dimethylformamide (DMF, AR), toluene (AR), tetrahydrofuran (THF, AR), dimethylsulfoxide (DMSO, AR), and methanol (AR) were purchased from Tianjin Damao Chemical Reagent Factory. Concentrated hydrochloric acid (37%), concentrated sulfuric acid (38%), phosphoric acid solution (38%) and glacial acetic acid (38%) were purchased from Chengdu Cologne Chemical Co. Carbon fiber, model T300, was purchased from Jiangsu Tianbird High-Tech Co. All solvents and chemicals were used as received without further purification.

2.2. Synthesis of 4-[3-(1,3-dioxolan-2-yl)-4-methoxystyryl]-4-methyl-2-[3-(1,3-dioxolan-2-yl) phenyl]-1,3-dioxolane and 2,2′-(1-Isopropyl-1,3-phenylene) bis[4-(furan-2-ylmethoxy) azetidine][3]

The dihydrazone-containing bisphenol structure, 4,4′-(-hydrazine-1,2-diylidenebis (methanylylidene)) bis (2-methoxyphenol) (abbreviated as HDP), was first synthesized following the route detailed in Scheme S1† (the structural characterization is shown in Fig. S1†). Subsequently, paraformaldehyde (9.6 g, 0.32 mol) and deionized water (17.84 g) were charged into a 250 mL round-bottom flask under a nitrogen atmosphere, where the pH was adjusted to 8–10 using dilute NaOH. The mixture was stirred in an oil bath at 40 °C for 30 min, after which HDP (24 g, 0.08 mol) and toluene (16 mL) were sequentially added. The temperature was gradually raised to 80 °C over 10 min, and the reaction proceeded at this temperature for 90 min with vigorous agitation. Finally, furfurylamine (15.52 g, 0.16 mol) was introduced via dropwise addition, and the reaction was continued at 80 °C for 6 hours. The crude product was washed three times with anhydrous ethanol and vacuum-dried at 60 °C to afford a light yellow powder (4-[3-(1,3-dioxolan-2-yl)-4-methoxystyryl]-4-methyl-2-[3-(1,3-dioxolan-2-yl) phenyl]-1,3-dioxolane, HDF) in 61% yield. The overall synthetic pathway is illustrated in Scheme 1a.

2,2′-(1-Isopropyl-1,3-phenylene) bis [4-(furan-2-ylmethoxy) azetidine] (BA-F) was prepared as a contrast. BA-F was prepared according to the method shown in Scheme 1b, which is slightly different from the reported synthesis.[52] First, bisphenol A (11.4 g, 0.05 mol) and toluene (30 ml) were added to a three-necked flask at room temperature. Subsequently, furfurylamine (9.7 g, 0.1 mol) was added dropwise at a rate of 1 s with stirring and finally paraformaldehyde (6 g, 0.2 mol) was added. The temperature was raised to 95 °C in a thermostatic oil bath with magnetic stirring for 6 hours. After the reaction was finished, the mixture was subjected to rotary evaporation for solvent removal, followed by dissolution in chloroform and subsequent re-evaporation. The resulting product was vacuum-dried to yield a milky white powder in 75% yield.

2.3. Preparation of HDF samples

An appropriate amount of DMF was added to a certain mass of HDF monomer. The mixture was ultrasonicated and then poured into a mold (80 mm × 10 mm × 4 mm). The samples were first placed in a vacuum oven at 120 °C for 1 hour to remove the solvent and obtain the prepolymer. Then the prepolymer was cured in a blower oven with a multi-step thermal curing process of 130 °C/2 h, 150 °C/2 h, 170 °C/2 h, and 190 °C/2 h. The samples were kept in the blower oven until cooling to room temperature. The resulting polymer, poly-(4-[3-(1,3-dioxolan-2-yl)-4-methoxystyryl]-4-methyl-2-[3-(1,3-dioxolan-2-yl) phenyl]-1,3-dioxolane) (PHDF), was thus obtained.

2.4. Preparation of HDF/CF composite samples

First, a PHDF prepolymer solution prepared by the aforementioned process was used for impregnation and the solution was uniformly applied to a carbon fiber fabric with a size of 50 mm × 50 mm. Afterwards, the solution-coated carbon fiber fabric was placed into a vacuum oven at 60 °C for 1 hour to remove most of the solvent. Finally, the pretreated material was transferred to a 120 °C blast oven for 1 hour to pre-cure the prepreg, and then the carbon fiber composite was produced by hot press curing using the curing process described above. The resulting material is the benzoxazine-based composite (referred to as PHDF/CF).

2.5. Characterization methods

The chemical structures of the monomers were characterized by ^{1}H and ^{13}C NMR spectroscopy using a Bruker TD-65536 NMR spectrometer (400 MHz) with deuterated chloroform (CDCl$_3$) and deuterated dimethyl sulfoxide (DMSO-d$_6$) as solvents. The chemical structure of the molecule was characterized by Fourier transform infrared (FTIR) spectroscopy using a Nicolet iS50 spectrometer (Thermo Fisher Scientific, USA) in attenuated total reflection (ATR) mode with a diamond anvil cell, where spectra were collected over 32 scans at a resolution of 4 cm^{-1} across the 4000–500 cm^{-1} range. The curing behavior of the monomers was analyzed by differential scanning calorimetry (DSC) using a Mettler Toledo DSC-3 instrument (Switzerland) under the following conditions: a heating rate of 10 °C min^{-1}, a temperature range of 50–350 °C, and a nitrogen flow rate of 50 mL min^{-1}. Thermal stability was evaluated by thermogravimetric analysis (TGA) using a Mettler Toledo TGA-2 analyzer (Switzerland) with identical heating parameters (10 °C min^{-1}, 50–800 °C, and 50 mL min^{-1} N$_2$ flow).
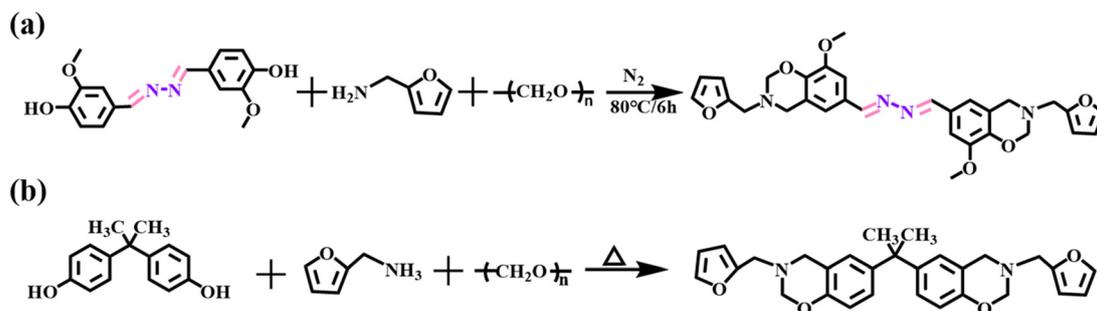
Scheme 1 Synthesis of (a) HDF and (b) BA-F monomers.

Combustion resistance was measured by microscale combustion calorimetry (MCC) using an FTT 0001 microcalorimeter (UK), employing a heating rate of 1 °C s^{-1} from 25–750 °C under an 80 mL min^{-1} nitrogen flow. Morphological analysis of pristine and recycled carbon fibers was conducted by scanning electron microscopy (SEM) using a JEOL JSM-7900F microscope. The tensile strengths of the virgin and regenerated carbon fibers were compared using an LLY-06EDC electronic single-fiber tensiometer. The chemical structures of the original and regenerated carbon fibers were tested using Raman spectroscopy (Horiba Labram HR Evolution, Japan). The laser energy was 12 mW and the wavelength was 532 nm.

The degradation performance of the resin was quantified using the 24-hour degradation ratio and degradation rate. For the degradation ratio test, resin samples were immersed in solvent for 24 hours. Every 2 hours, fragments were retrieved, wiped, dried, and weighed to record mass loss. Carbon fiber recycling efficiency was assessed by comparing the morphologies, mechanical properties, and chemical structures of virgin and recycled fibers. Specifically, PHDF/CF composite strips (10 × 30 mm) were degraded in 20 mL of degradation solution at 50 °C. The time required for fiber recovery was determined by monitoring carbon fiber weight loss. During degradation, samples were extracted every 2 hours, dried, and weighed to establish a correlation between the mass loss of composite strips and the degradation time.

3. Results and discussion

3.1. Chemical structures of HDF and BA-F

The chemical structure of HDF was confirmed by ^{1}H NMR and ^{13}C NMR spectroscopy. In the ^{1}H NMR spectrum (Fig. 1a), the signal at 3.70 ppm was assigned to the methylene hydrogen

(e-H) bridging the oxazine and furan rings, while the peak at 3.98 ppm corresponded to the methoxy group hydrogen (b-H) on the benzene ring.[53,54] The peak of N-CH$_2$-Ar hydrogen (c-H) in the oxazine ring appeared at 4.08 ppm and that of the Ar-O-CH$_2$ hydrogens (d-H) was observed at 5.07 ppm.[54] Aromatic hydrogens in the benzene and furan rings resonated between 6.27 and 7.42 ppm, and the distinctive peak at 8.57 ppm was attributed to the hydrogen (a-H) on the carbon linking the benzene ring to the dihydrazone bond.[48] In the ^{13}C NMR spectrum (Fig. 1d), the carbon (a-C) bonded to both the benzene ring and the dihydrazone group resonated at 148.2 ppm,[48] whereas the N-CH$_2$-Ar carbon (c-C) appeared at 58.4 ppm.[54] The methoxy group carbon (b-C) on the benzene ring was detected at 56.0 ppm, and the Ar-O-CH$_2$ carbon (d-C) exhibited a signal at 82.9 ppm.[53]

The successful synthesis of HDF was further confirmed by FT-IR spectroscopy (Fig. 1c). The characteristic absorption peak at 921 cm^{-1} corresponds to the stretching vibration of the oxazine ring,[55] while the symmetric and antisymmetric vibrations of Ar-O-CH$_2$ in the oxazine ring were observed at 1025 cm^{-1} and 1223 cm^{-1}, respectively.[56] Simultaneously, the symmetric and antisymmetric vibrations of N-CH$_2$-Ar within the oxazine ring appeared at 1127 cm^{-1} and 1375 cm^{-1}, and the benzene ring skeleton vibration was identified at 1190 cm^{-1}.[14,54] Notably, the furan ring exhibited a stretching vibration peak at 1582 cm^{-1},[53] and the C=N–C=N bond vibration was detected at 1622 cm^{-1}.[48] Additionally, the stretching vibration peak of the C–H of the furan ring (3115 cm^{-1}) and the characteristic absorption peak of the C–O–C of the furan ring (1072 cm^{-1}) were observed in the figure,[53,57] collectively validating the molecular structure of HDF.

The chemical structure of BA-F was confirmed by ^{1}H NMR, ^{13}C NMR, and FT-IR spectroscopy (Fig. 1b–f). In the ^{1}H NMR
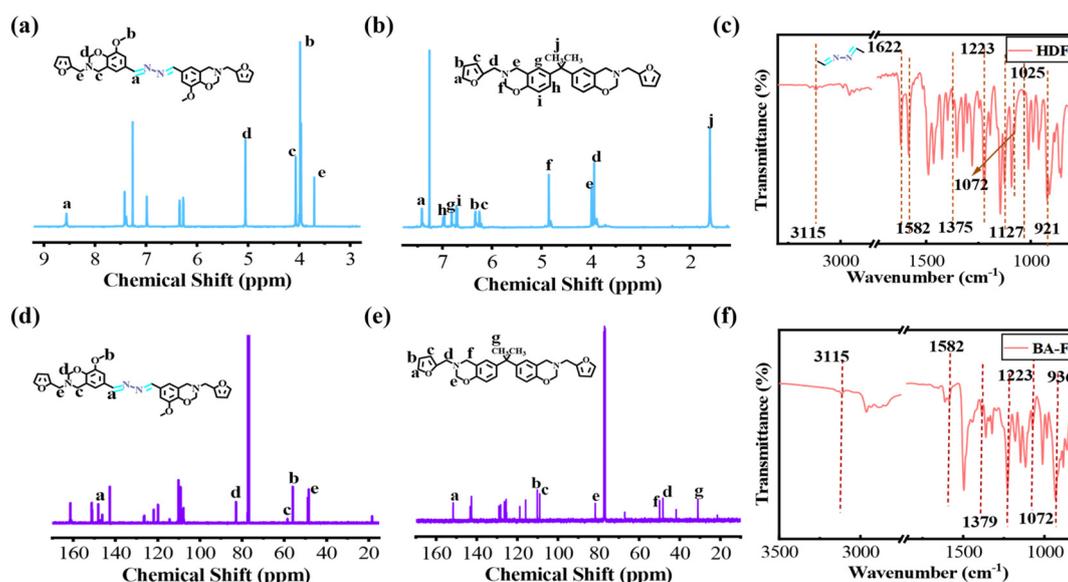

Fig. 1 ^{1}H NMR spectra of HDF (a) and BA-F (b); ^{13}C NMR spectra of HDF (d) and BA-F (e); and FTIR spectra of HDF (c) and BA-F (f).

spectrum (Fig. 1b), the methyl group hydrogen (j-H) exhibited a characteristic peak at 1.6 ppm, while the methylene hydrogen (d-H) bridging the oxazine and furan rings resonated at 3.9 ppm. The N-CH$_2$-Ar hydrogen (f-H) in the oxazine ring appeared at 4.8 ppm, and the Ar-O-CH$_2$ hydrogen (e-H) was observed at 4.0 ppm. Aromatic hydrogens on the benzene and furan rings generated signals between 6.2 and 7.4 ppm, with the solvent (deuterated chloroform) peak detected at 7.2 ppm.[52,58] In the ^{13}C NMR spectrum (Fig. 1e), key carbon assignments included: 21.5 ppm for the methyl group (g-C), 48.3 ppm for the CH$_2$-N carbon (d-C), 49.9 ppm for the N-CH$_2$-Ar carbon (f-C), 81.6 ppm for the Ar-O-CH$_2$ carbon (e-C), and 109–142 ppm for the furan ring carbons (a-C, b-C, and c-C).[52,58] The FT-IR spectrum (Fig. 1f) further validated the structure, with characteristic absorptions at 936 cm^{-1} (oxazine ring), 1023 cm^{-1} and 1072 cm^{-1} (symmetric/antisymmetric vibrations of Ar-O-CH$_2$), 1379 cm^{-1} (N-CH$_2$-Ar), and 1582 cm^{-1} and 3115 cm^{-1} (C–H stretching of the furan ring).[57,58] It is notable that the absorption peak of C–O–C in the furan ring overlaps with the characteristic peak of Ar-O-CH$_2$ in the oxazine ring at 1072 cm^{-1}. These data collectively confirm the successful synthesis of BA-F.

3.2. Curing mechanism of HDF

The curing behavior of the HDF monomer was analyzed by DSC and compared with that of BA-F and the results are shown in Fig. 2a and Table 1. The HDF monomer exhibited lower ring-opening polymerization temperatures, with an onset of 212.5 °C

Table 1 DSC analysis results of HDF and BA-F

Sample	T_{oneset} (°C)	T_{peak} (°C)	ΔH (J g^{-1})
HDF	212.5	227.3	99.0
BA-F	214.3	260.0	221.8

and a peak at 227.3 °C, compared to the BA-F monomer, which demonstrated higher values of 214.3 °C (onset) and 260.0 °C (peak). The enthalpy of HDF (99.0 J g^{-1}) was much lower than that of BA-F (221.8 J g^{-1}). It can be inferred that the dihydrazone bond (C=N–N=C) can promote the ring-opening reaction of benzoxazines and decrease the enthalpy.

In order to further study the curing mechanism of HDF and BA-F monomers, FTIR was used to characterize the samples after curing at different temperatures, and the results are shown in Fig. 2b and S2.† For HDF (Fig. 2b), characteristic absorption peaks at 921 cm^{-1} (oxazine ring), 1127 cm^{-1} (Ar-CH$_2$-N) and 1223 cm^{-1} (Ar-O-C) completely disappeared after 1 hour of curing at 190 °C, confirming full ring-opening of the oxazine structure in HDF. Notably, the pronounced spectral changes observed in the oxazine-related peaks before and after 190 °C curing may be attributed to the rigid conjugated dihydrazide groups inherent to the HDF structure. In the temperature gradient curing FTIR spectrum of BA-F (Fig. S2†), the intensity of characteristic absorption peaks such as 936 cm^{-1} (oxazine ring), 1072 cm^{-1} (Ar-O-CH$_2$) and 1379 cm^{-1} (Ar-CH$_2$-N) gradually decreased from 160 °C, indicating partial ring-
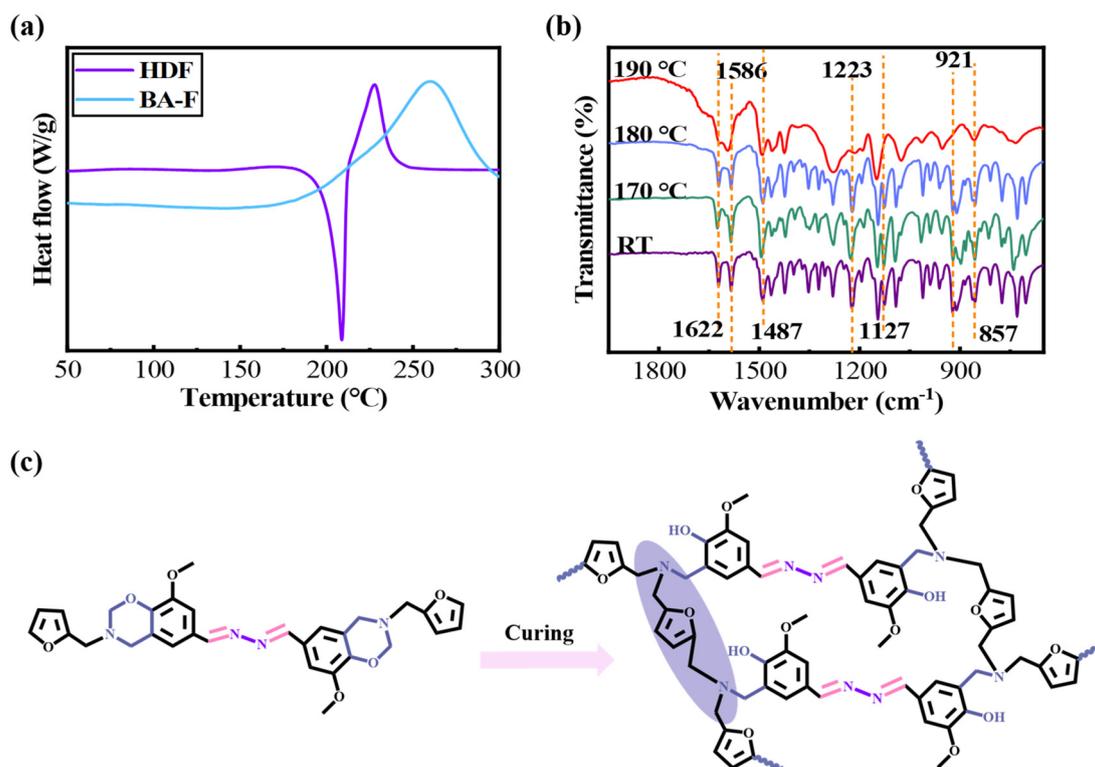

Fig. 2 (a) DSC curves of HDF *vs.* BA-F; (b) FTIR spectra of HDF at different stages; and (c) curing mechanism of PHDF.

opening of the oxazine ring in BA-F. By 200 °C, these peaks completely disappear, demonstrating complete ring-opening of the oxazine ring in BA-F. Concurrently, the disappearance of tri-substituted benzene ring vibrations (814 cm^{-1} and 1494 cm^{-1}) and the emergence of tetra-substituted counterparts (857 cm^{-1} and 1479 cm^{-1})[55,59] confirmed Mannich bridge formation.[60] Significantly, in the infrared spectrum of HDF (Fig. 2b), no conversion of the three-substituted benzene ring into the four-substituted benzene ring was observed. This is mainly because in the structure of HDF, the benzene ring is originally a tetrasubstituted benzene ring (1487 cm^{-1} and 857 cm^{-1}),[55,59] so no similar structural transformation occurs during the curing process. In addition, during the heating process, the absorption peak intensity of the two monomers at 1586 cm^{-1} showed the same change (both widened), which confirmed the involvement of furan rings in the polymerization process.[14] Based on these findings, the possible curing mechanism of HDF and BA-F monomers was proposed, as shown in Fig. 2c and S3.†

3.3. Thermal properties of HDF

The thermal stability of PHDF and PBA-F under an N$_2$ atmosphere was measured and analyzed by TGA. The results are shown in Fig. 3a and Table 2. The results showed that the temperature at 5% weight loss ($T_{d5\%}$) and the temperature at 10% weight loss ($T_{d10\%}$) of PHDF were 289 °C and 331 °C, respectively, both lower than those of PBA-F (325 °C for $T_{d5\%}$ and 386 °C for $T_{d10\%}$). This is attributed to the relatively weak bond energy of the dynamic covalent dihydrazone bonds, which undergo decomposition as temperature increases. However, PHDF exhibits a higher 30% weight loss temperature ($T_{d30\%}$ = 518 °C) compared to PBA-F ($T_{d30\%}$ = 471 °C). The enhanced high-temperature stability arises from the self-crosslinking of aromatic Schiff base structures, forming thermally stable nitrogen-containing six-membered rings. These rings further transform into dense carbon layers during pyrolysis, acting as a thermal barrier to suppress degradation.[41,61] Consequently, the residual carbon rate of PHDF is 59.5% at 800 °C, which is higher than that of PBA-F (51.5% at 800 °C).

Table 2 Thermal performance data of PHDF and PBA-F

Sample	$T_{d5\%}$ (°C)	$T_{d10\%}$ (°C)	$T_{d30\%}$ (°C)	Char yield (wt%)
PHDF	289	331	518	59.5
PBA-F	325	386	471	51.5

Table 3 MCC test results of PHDF and PBA-F

Sample	HRC (J g^{-1} K^{-1})	THR (kJ g^{-1})	T_{max} (°C)	PHRR (W g^{-1})
PHDF	31.2	2.2	330.0	31.5
PBA-F	100.1	7.7	407.6	101.1

These results indicate that the introduction of rigid conjugated dihydrazone groups into the cross-linked structure enhances the thermal stability of the resin.

The flame-retardant properties of PHDF and PBA-F were evaluated using microscale combustion calorimetry (MCC) (Fig. 3b and Table 3).[62] The peak heat release rate (PHRR) of PHDF (31.5 W g^{-1}) was 3.2 times lower than that of PBA-F (101.1 W g^{-1}), while its total heat release (THR = 2.2 kJ g^{-1}) and heat release capacity (HRC = 100.1 J g^{-1} K^{-1}) were also significantly reduced compared to those of PBA-F (THR = 7.7 kJ g^{-1} and HRC ≈ 320 J g^{-1} K^{-1}). This difference primarily stems from the flame-retardant properties of PHDF under high-temperature conditions. The dynamic dihydrazone bonds undergo decomposition upon heating, triggering self-crosslinking of aromatic Schiff base segments to form nitrogen-containing six-membered rings.[41] These structures further transform into a dense carbon layer during pyrolysis, effectively blocking heat transfer and suppressing flame spread. In addition, according to the literature report,[52] the ultimate oxygen index of benzoxazine resins with furan rings is higher than 26%, which has certain advantages for flame retardancy.

3.4. Degradation properties of HDF

3.4.1. Selection of solvent for degradation. To identify an optimal degradation solvent, the dissolution and degradation
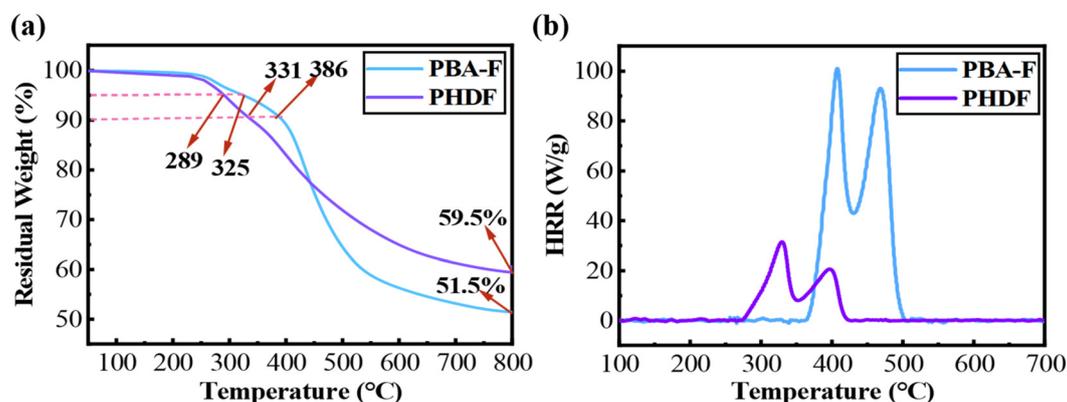

Fig. 3 (a) TGA plots of PHDF and PBA-F under a nitrogen atmosphere; (b) MCC test curves of the two resins.

rates of HDF in six aqueous–organic solvent mixtures (2 : 8 v/v) were systematically compared. The solubility of PHDF fragments (approximately 0.3 g) was evaluated by immersing them in selected organic solvents—including methanol, ethanol, tetrahydrofuran, dimethyl sulfoxide, *N*,*N*-dimethylformamide, acetone, and distilled water (as a control)—at room temperature for 24 hours. Finally, the resin fragments were taken out and the changes in solution color were observed (Fig. 4a) (see Fig. S3† for the complete picture). In Fig. 4a, the color of the solution and the size of the resin fragments had not changed significantly after the fragments were placed in five kinds of solutions (methanol, ethanol, tetrahydrofuran, dimethyl sulfoxide, *N*,*N*-dimethylformamide and acetone). However, when the resin was immersed in a solution of water and acetone (2/8, v/v), the color of the solution changed. A water–acetone mixture (2 : 8, v/v) was initially selected as the degradation medium. To validate its efficacy, the degradation rates of PHDF in 0.1 M HCl aqueous solutions containing various organic co-solvents were systematically compared at 50 °C (Fig. 4d). The water–acetone system exhibited the fastest degradation rate of ~2 mg h^{-1}, surpassing other solvent combinations. This accelerated degradation is attributed to acetone's enhanced solvation capacity and synergistic interaction with water, which facilitates polymer chain scission. Consequently, the water–acetone mixture was confirmed as the optimal degradation solution for efficient resin decomposition.

To optimize the acetone–water ratio in the degradation solution, both visual and dissolution phenomena (Fig. 4b) (see Fig. S4† for the complete picture) were systematically compared across different solvent ratios. As shown in Fig. 4b, distinct color changes occurred in solutions with acetone-to-water ratios of 3 : 7, 2 : 8, and 1 : 9 (v/v), with the most pronounced change observed for the 2 : 8 (v/v) mixture. Although dissolution rates across these three ratios exhibited minimal variation (Fig. 4e), the 2 : 8 (v/v) acetone–water system was ultimately selected due to its optimal balance of visible reactivity

and efficient degradation performance. After removing the fragments from the small volumetric flask, they were briefly dried and weighed, and the swelling rate (SR) was calculated using the formula:

$$\text{SR} = \frac{m_1 - m_0}{m_0} \times 100\% \tag{1}$$

The swelling rate is calculated by measuring the mass difference of resin fragments before and after swelling, where m_0 denotes the initial dry mass (g) of the resin fragments and m_1 represents their mass (g) post-swelling. This parameter quantitatively reflects the material's capacity to absorb solvent during the swelling process. As shown in Fig. 4c and e, the resin exhibited a maximum swelling rate of less than 20% across all tested solvents, with significant variations observed depending on the solvent type. Concurrently, Fig. 4a demonstrates that the solvent color remained unchanged after 24-hour immersion in most aqueous solvent mixtures, indicating minimal chemical interaction between the resin and solvents. These combined results highlight the material's exceptional solvent resistance, characterized by low swelling propensity and structural stability in diverse liquid environments.

3.4.2. Factors affecting degradation. The degradation behavior of PHDF resin was systematically investigated under varying conditions (temperature, acid concentration, and solvent ratios), as illustrated in Fig. 5a–d. Dihydrazone-based dynamic bonds, known to degrade under multiple environmental factors,[48] were evaluated through four experimental groups to identify optimal degradation parameters. Comparative studies revealed that degradation rates in 0.1 M HCl/acetone–water (2 : 8, v/v) solutions at 50 °C were significantly faster than those at 23 °C. Furthermore, increasing HCl concentration accelerated bond cleavage, with the fastest degradation observed in the 0.1 M HCl/acetone–water (2 : 8, v/v) system. Additional tests across solvent ratios (10 : 0–1 : 9, v/v) at 50 C confirmed that the 2 : 8 (v/v) acetone–water mixture
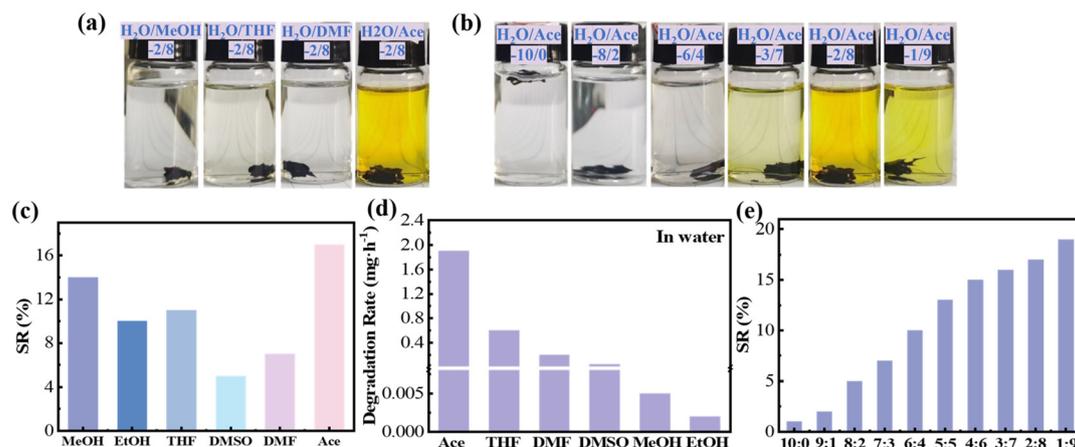
Fig. 4 (a) Dissolution experiments of PHDF in different solvents (water/MeOH, EtOH, THF, DMSO, and DMF) in a ratio of 2/8 at room temperature; (b) dissolution experiments of PHDF in a ratio of water/acetone from 10/0 to 1/9 at room temperature; (c) dissolution rate of PHDF at room temperature in water with different solvents (2/8); (d) degradation rate of PHDF in 0.1 M HCl water/primary solvent (2/8, v/v) at 50 °C; and (e) degradation rate of PHDF in water with different ratios of acetone.
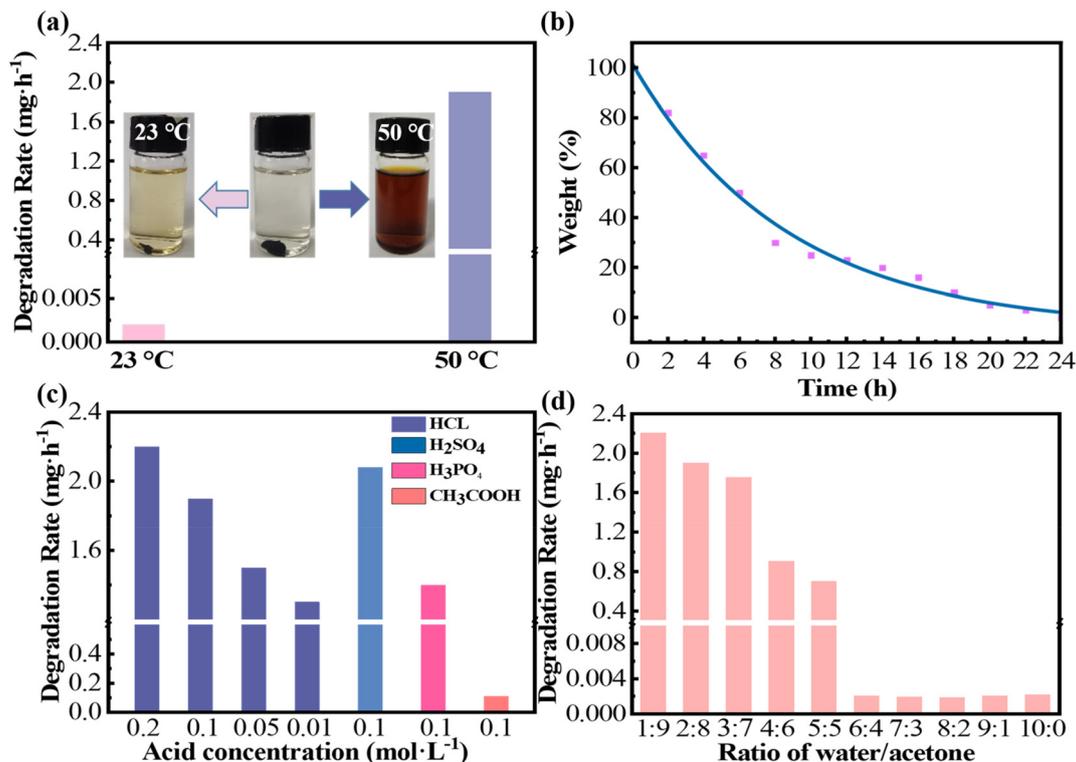
Fig. 5 (a) Different degradation rates in 0.1 M HCl water/acetone (2/8, v/v) solution at 23 °C and 50 °C; (b) plot of weight change of PHDF in 0.1 M HCl/acetone at 50 °C over time; (c) degradation rates in different acidic water/acetone (2/8, v/v) solutions at 50 °C; and (d) degradation rates in 0.1 M HCl water/acetone solution at 50 °C.

maximized the degradation efficiency. These results demonstrate that elevated temperature, controlled acidity, and solvent polarity synergistically enhance the breakdown of PHDF's dynamic network.

3.4.2.1. Effect of temperature. The degradation behavior of PHDF fragments was evaluated in 0.1 M HCl/acetone–water (2 : 8, v/v) solutions at 25 °C and 50 °C (Fig. 5a). At 50 °C, the resin fragments degraded almost completely within 24 hours, dissolving fully into the solution, whereas minimal degradation (<1%) occurred at 23 °C over the same duration. Degradation rates exhibited a stark temperature dependence: 1.898 mg h^{-1} at 50 °C *versus* 0.002 mg h^{-1} at 23 °C. To further characterize the time-dependent degradation profile at 50 °C, the mass loss of PHDF fragments was monitored (Fig. 5b). Remarkably, 80% of the resin degraded within the first 12 hours, achieving full decomposition within 24 hours. These results conclusively demonstrate that PHDF degradation is highly temperature-sensitive, with accelerated bond cleavage under elevated thermal conditions.

3.4.2.2. Effect of acid class and concentration. The degradation behavior of PHDF in 0.1 M aqueous acetone (2 : 8, v/v) solutions containing HCl, H$_2$SO$_4$, H$_3$PO$_4$, or CH$_3$COOH was systematically evaluated at 50 °C (Fig. 5c). Under identical concentration and temperature conditions, strong acids exhibited significantly higher degradation rates (2.1 mg h^{-1} for H$_2$SO$_4$ and 1.9 mg h^{-1} for HCl) compared to weak acids (1.4 mg h^{-1}

for H$_3$PO$_4$ and 0.1 mg h^{-1} for CH$_3$COOH), confirming a direct correlation between H$^+$ concentration and degradation efficiency. To optimize reaction parameters while minimizing byproduct formation and operational costs, HCl was selected for further investigation of proton-driven dihydrazone bond cleavage. As shown in Fig. 5c, increasing HCl concentration progressively enhanced catalytic activity at 50 °C, demonstrating that elevated H$^+$ availability accelerates bond scission. These results highlight the critical role of proton concentration in governing the temperature-dependent degradation kinetics of PHDF.[63,64]

3.4.2.3. Effect of different ratios of water/acetone solvents. The influence of water/acetone ratios on PHDF degradation was investigated in 0.1 M HCl at 50 °C across solvent compositions ranging from 1 : 9 to 10 : 0 (v/v, water/acetone) (Fig. 5d). The degradation rate peaked at 2.2 mg h^{-1} for the 1 : 9 (v/v) ratio and 1.9 mg h^{-1} for the 2 : 8 (v/v) system. However, increasing water content above 60% (v/v) drastically reduced the degradation efficiency, with negligible degradation observed in water-dominant solutions (>6 : 4 ratio). This decline correlates with the reduced solubility of degradation byproducts and diminished polymer wettability in high-water-content environments.[63,64] These results demonstrate that acetone-rich solutions enhance degradation kinetics by promoting solvent penetration and fragment dissolution, highlighting the critical role of solvent polarity in governing PHDF decomposition.

Based on systematic investigation of degradation parameters, the optimal conditions for PHDF decomposition were identified as a 0.1 M HCl/acetone–water (2 : 8, v/v) system at 50 °C, which exhibited the highest degradation rate. This solvent–environment combination was consequently selected for resin decomposition in fiber-reinforced composite recycling, leveraging its balanced solvent polarity and proton concentration to maximize bond cleavage efficiency while maintaining process controllability. The accelerated degradation kinetics under these conditions ensure rapid resin removal without compromising the structural integrity of recycled fibers, demonstrating practical applicability in sustainable material recovery processes.

3.4.3. Degradation mechanism. The HDF framework incorporates a Schiff base structure—a dynamic covalent network characterized by reversible C=N bonds.[65,66] These pH-responsive linkages undergo acid-catalyzed hydrolysis, dissociating reversibly into precursor amine and aldehyde groups while retaining structural adaptability.[48] This unique dual functionality allows precise regulation of degradation kinetics through environmental stimuli, such as acidic conditions, enabling customizable material lifespans in recyclable polymer systems. The equilibrium between bond reformation and cleavage not only facilitates controlled degradation but also supports potential monomer recovery, positioning such architectures as critical tools for sustainable material design.

FT-IR analysis of the PHDF degradation solution (Fig. 6a and b) revealed a broad absorption peak at 1682 cm^{-1}, corresponding to aldehyde (C=O) stretching vibrations, alongside the disappearance of the C=N peak at 1622 cm^{-1}. These observations confirm the degradation mechanism (Fig. 6c).

Under acidic conditions, the Schiff base structure hydrolyzes into aldehyde groups, disrupting the three-dimensional cross-linked network and generating soluble oligomers. The dissolution of these oligomers in organic solvents underscores the system's capacity for controlled disassembly.

The dihydrazone bonds in PHDF degrade *via* a two-step acid-catalyzed process.[48] Initially, hydrolysis converts dihydrazone structures into mono-hydrazone intermediates, which subsequently undergo further cleavage. This stepwise mechanism enables rapid and complete degradation in the presence of excess acid, highlighting the exceptional acid sensitivity of hydrazone groups. During degradation, covalent adaptive networks (CANs) first fragment into oligomers dissolved in the solution. Prolonged exposure further breaks down residual dihydrazone bonds in these oligomers, demonstrating a hierarchical disassembly process driven by bond lability under acidic conditions.

The fully cured PBA-F resin fragments were placed in 1 M HCl water/acetone (2/8, v/v) mixed solution at room temperature and in a blast oven at 50 °C for 24 hours. To confirm the critical role of dihydrazone bonds in PHDF degradation, control experiments were conducted using fully cured PBA-F resin fragments—a structural analog lacking dihydrazone bonds—in 1 M HCl/acetone–water (2 : 8, v/v) under two conditions: 23 °C (ambient) and 50 °C (forced-air oven) for 24 hours (Fig. 6d). Temperature induced neither decomposition nor solution discoloration, demonstrating PBA-F's stability. Comparative structural analysis (Scheme 1a and b) revealed two key distinctions: (1) HDF contains a central dihydrazone bond, while BA-F has a non-degradable carbon chain; (2) HDF features a methoxy group on the aromatic ring, which
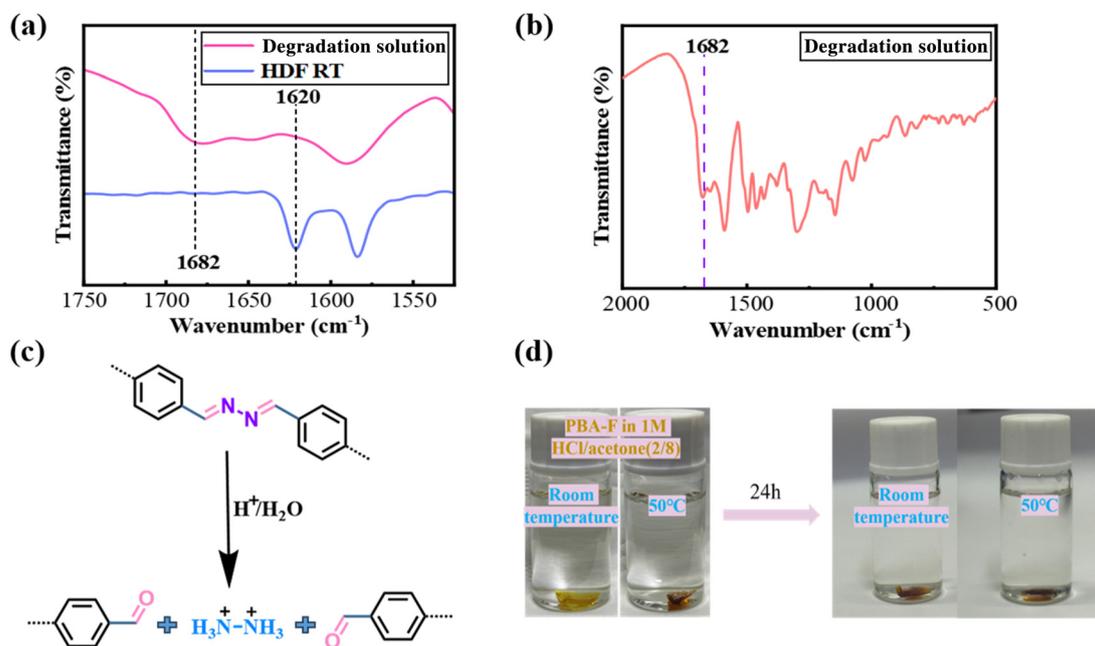

Fig. 6 (a) and (b) Infrared spectra after degradation of PHDF; (c) degradation mechanism of PHDF; and (d) images of PBA-F placed in 1 M HCl water/acetone (2/8, v/v) solution at room temperature and 50 °C for 24 h.

is absent in BA-F. Given methoxy groups' inherent stability under acidic conditions, this contrast conclusively attributes PHDF's degradability to its dihydrazone bonds rather than peripheral substituents. These results establish dihydrazone bonds as indispensable acid-labile units enabling controlled polymer disassembly.

3.5. Recyclability of carbon fiber-reinforced HDF composites

The carbon fiber (CF)-reinforced composites fabricated with PHDF resin were subjected to controlled degradation to evaluate their carbon fiber recovery (Fig. 7a). Composite specimens (10 mm × 30 mm) were immersed in 20 mL of 0.1 M HCl/acetone–water solution (2 : 8, v/v) within glass vials and maintained at 50 °C in a thermal chamber. Throughout the 24-hour process, real-time monitoring captured the progressive disintegration of the polymer matrix and the corresponding solution changes (Fig. 7a and b). The degradation protocol successfully separated CF bundles from the resin while preserving fiber integrity, demonstrating PHDF's suitability for circular composite manufacturing through acid-triggered matrix dissolution.

As shown in Fig. 7a, after 12 hours, the color of the mixed solution appeared yellow, uniform and transparent, without granular matter. The carbon fiber picked up by tweezers was deformed, bent, and separated easily. As shown in Fig. 7b, the weight of the composite decreased to 80% after 10 hours. After 12 hours, the weight further decreased to 76%, which indicates that the resin matrix can be completely degraded in 12 hours.

To assess the impact of the degradation process on carbon fibers (CFs), comprehensive analyses were performed to compare the surface morphologies, chemical structures, and mechanical performance of pristine and recycled fibers. Scanning electron microscopy (SEM) images (Fig. 7c) revealed
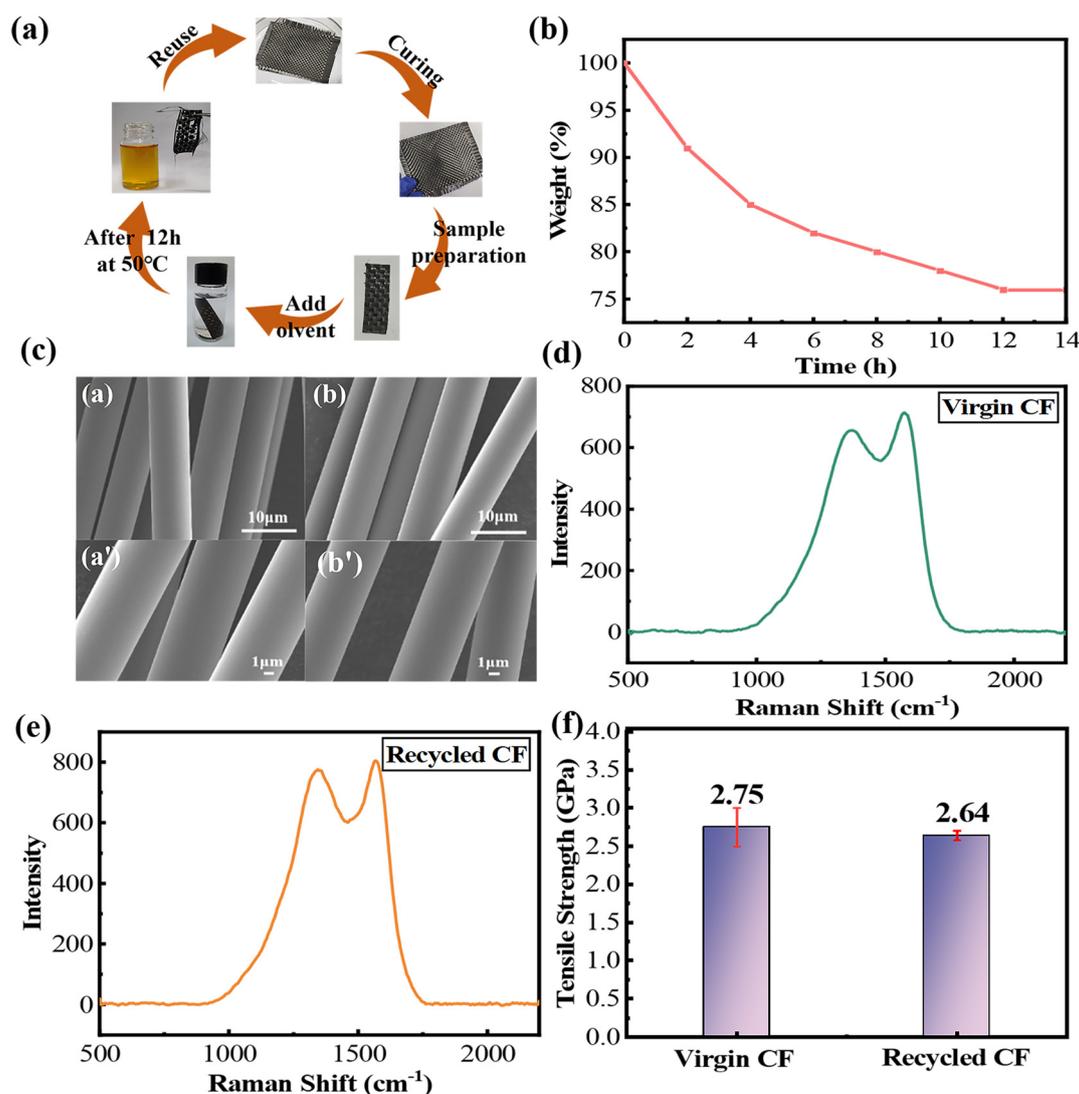

Fig. 7 (a) Schematic diagram of degradation of PHDF/CF in 0.1 M HCl water/acetone (2/8, v/v); (b) weightlessness diagram of the CF-reinforced composite; (c) (a and a′) SEM images of raw carbon fiber and (b and b′) recycled carbon fiber; (d) and (e) Raman spectra of virgin and recycled carbon fibers; and (f) monofilament tensile strength and elongation at break of virgin and recycled carbon fibers.

that the recycled CFs retained smooth surfaces without cracks or pitting, with diameters nearly identical to those of untreated fibers. Raman spectroscopy (Fig. 7d and e) demonstrated comparable D/G peak intensity ratios between the materials—1.52 for pristine fibers and 1.44 for recycled fibers—indicating minimal structural damage during degradation. Monofilament tensile testing further confirmed mechanical integrity, with recycled CFs achieving 2.64 GPa strength (96% of pristine fibers' 2.75 GPa) (Fig. 7f). These combined results demonstrate that the HCl/acetone–water degradation system effectively separates resin matrices while preserving the CF morphology, chemical stability, and critical mechanical properties, enabling high-value fiber recovery for sustainable composite recycling.

4. Conclusion

In this study, a novel molecular design strategy was developed for recyclable fiber composites by incorporating acid-labile dihydrazone bonds into benzoxazine resins, enabling controlled matrix degradation. The synthesized PHDF resin demonstrated exceptional thermal stability with a 59.5% char residue at 800 °C and superior flame retardancy, exhibiting a low heat release capacity (31.2 J g^{-1} K^{-1}), total heat release (2.2 kJ g^{-1}), and peak heat release rate (31.5 W g^{-1}). Systematic optimization of degradation parameters revealed that temperature, solvent composition, and acidity significantly influenced degradation rates. The optimal conditions—0.1 M HCl in acetone–water (2 : 8, v/v) at 50 °C—achieved a degradation rate of 1.89 mg h^{-1} within 24 hours while preserving carbon fiber (CF) integrity. Recycled CFs retained a smooth surface morphology and 96% of the original tensile strength (2.64 vs. 2.75 GPa), with Raman spectroscopy confirming structural preservation (D/G ratio: 1.44 vs. 1.52). These combined properties position PHDF as a promising matrix for sustainable composites, balancing high-temperature performance, degradability and high-value fiber recovery for circular manufacturing.

Conflicts of interest

There are no conflicts to declare.

Data availability

The data are available from the corresponding author on reasonable request.

Acknowledgements

References

1 A. Tarek, L. Jia, G. Robert and I. Hatsuo, *Benzoxazole Resin: A Novel Class of Thermoset Polymer via Smart Benzoxazine Resin*, 2012.

2 P. Froimowicz, C. R. Arza, L. Han and H. Ishida, Smart, sustainable, and ecofriendly chemical design of fully bio–based thermally stable thermosets based on benzoxazine chemistry, *ChemSusChem*, 2016, **9**(15), 1921–1928.

3 I. Machado, C. Shaer, K. Hurdle, V. Calado and H. Ishida, Towards the development of green flame retardancy by polybenzoxazines, *Prog. Polym. Sci.*, 2021, **121**, 101435.

4 W. Wang, J. Jiang, Q. An, R. Shi, S. Shao and Z. Wang, Preparation and Performances of Degradable Polybenzoxazine by Ring-Opening Metathesis Polymerization, *ACS Sustainable Chem. Eng.*, 2023, **11**(39), 14622–14632.

5 T. Takeichi and T. Agag, High performance polybenzoxazines as novel thermosets, *High Perform. Polym.*, 2006, **18**(5), 777–797.

6 C. J. Moore, Synthetic polymers in the marine environment: a rapidly increasing, long-term threat, *Environ. Res.*, 2008, **108**(2), 131–139.

7 Y. Lu, Y. Zhang and K. Zhang, Renewable biomass resources to access halogen-and phosphorus-free flame retardant thermosets with ultra-low heat release capacity, *Chem. Eng. J.*, 2022, **448**, 137670.

8 J. Podschun, A. Stücker, R. I. Buchholz, M. Heitmann, A. Schreiber, B. Saake and R. Lehnen, Phenolated lignins as reactive precursors in wood veneer and particleboard adhesion, *Ind. Eng. Chem. Res.*, 2016, **55**(18), 5231–5237.

9 C. E. Okonkwo, S. Z. Hussain, H. Onyeaka, A. A. Adeyanju, C. O. Nwonuma, A. A. Bashir, A. Farooq, C. Zhou and T. D. Shittu, Lignin polyphenol: From biomass to innovative food applications, and influence on gut microflora, *Ind. Crops Prod.*, 2023, **206**, 117696.

10 D. Xu, C. Lou, J. Huang, X. Lu, Z. Xin and C. Zhou, Effect of inhibitor-loaded halloysite nanotubes on active corrosion protection of polybenzoxazine coatings on mild steel, *Prog. Org. Coat.*, 2019, **134**, 126–133.

11 B. Lochab, I. K. Varma and J. Bijwe, Cardanol-based bis-benzoxazines: effect of structure on thermal behaviour, *J. Therm. Anal. Calorim.*, 2012, **107**(2), 661–668.

12 L. Puchot, P. Verge, T. Fouquet, C. Vancaeyzeele, F. Vidal and Y. Habibi, Breaking the symmetry of dibenzoxazines: a paradigm to tailor the design of bio-based thermosets, *Green Chem.*, 2016, **18**(11), 3346–3353.

13 F. Liaqat, L. Xu, M. I. Khazi, S. Ali, M. U. Rahman and D. Zhu, Extraction, purification, and applications of vanillin: A review of recent advances and challenges, *Ind. Crops Prod.*, 2023, **204**, 117372.

14 P. Thirukumaran, A. Shakila Parveen and M. Sarojadevi, Synthesis and copolymerization of fully biobased benzoxazines from renewable resources, *ACS Sustainable Chem. Eng.*, 2014, **2**(12), 2790–2801.

15 C. Wang, J. Sun, X. Liu, A. Sudo and T. Endo, Synthesis and copolymerization of fully bio-based benzoxazines from guaiacol, furfurylamine and stearylamine, *Green Chem.*, 2012, **14**(10), 2799–2806.

16 R. Yang, M. Han, B. Hao and K. Zhang, Biobased high-performance tri-furan functional bis-benzoxazine resin derived from renewable guaiacol, furfural and furfurylamine, *Eur. Polym. J.*, 2020, **131**, 109706.

17 F. Hong, C. Qu and L. Wang, Cerium improves growth of maize seedlings via alleviating morphological structure and oxidative damages of leaf under different stresses, *J. Agric. Food Chem.*, 2017, **65**(41), 9022–9030.

18 Y. Zhang, F. Seidi, M. Ahmad, L. Zheng, L. Cheng, Y. Huang and H. Xiao, Green and sustainable natural derived polysulfides for a broad range of applications, *Green Chem.*, 2023, **25**(17), 6515–6537.

19 G. Lligadas, A. Tüzün, J. C. Ronda, M. Galià and V. Cádiz, Polybenzoxazines: new players in the bio-based polymer arena, *Polym. Chem.*, 2014, **5**(23), 6636–6644.

20 L. Dumas, L. Bonnaud, M. Olivier, M. Poorteman and P. Dubois, Eugenol-based benzoxazine: from straight synthesis to taming of the network properties, *J. Mater. Chem. A*, 2015, **3**(11), 6012–6018.

21 J. R. Oliveira, L. R. V. Kotzebue, D. B. Freitas, A. L. A. Mattos, A. E. da Costa Júnior, S. E. Mazzetto and D. Lomonaco, Towards novel high-performance bio-composites: Polybenzoxazine-based matrix reinforced with Manicaria saccifera fabrics, *Composites, Part B*, 2020, **194**, 108060.

22 C. Peng, Z. Wu and D. Zhou, Synthesis of a benzoxazine-type dispersant and its application on epoxy/benzoxazine/ZrO2 composite: Dispersion performance and tensile behavior, *Composites, Part B*, 2019, **167**, 507–516.

23 K. Zhang, Y. Liu and H. Ishida, Polymerization of an AB-type benzoxazine monomer toward different polybenzoxazine networks: When diels–alder reaction meets benzoxazine chemistry in a single-component resin, *Macromolecules*, 2019, **52**(19), 7386–7395.

24 Y. Liu, L. Yuan, G. Liang and A. Gu, Preparation of thermally resistant and mechanically strong biomass benzoxazine resins via green strategy, *ACS Sustainable Chem. Eng.*, 2024, **12**(3), 1247–1254.

25 R. Yang, N. Li, C. J. Evans, S. Yang and K. Zhang, Phosphaphenanthrene-functionalized benzoxazines bearing intramolecularly hydrogen-bonded phenolic hydroxyl: synthesis, structural characterization, polymerization mechanism, and property investigation, *Macromolecules*, 2023, **56**(4), 1311–1323.

26 J. Dai, N. Teng, Y. Peng, Y. Liu, L. Cao, J. Zhu and X. Liu, Biobased benzoxazine derived from daidzein and furfurylamine: microwave–assisted synthesis and thermal properties investigation, *ChemSusChem*, 2018, **11**(18), 3175–3183.

27 X. Liu, R. Zhang, T. Li, P. Zhu and Q. Zhuang, Novel fully biobased benzoxazines from rosin: synthesis and properties, *ACS Sustainable Chem. Eng.*, 2017, **5**(11), 10682–10692.

28 X. Shen, J. Dai, Y. Liu, X. Liu and J. Zhu, Synthesis of high performance polybenzoxazine networks from bio-based furfurylamine: Furan vs benzene ring, *Polymer*, 2017, **122**, 258–269.

29 H. Ding, X. Wang, L. Song and Y. Hu, Recent advances in flame retardant bio-based benzoxazine resins, *J. Renewable Mater.*, 2022, **10**(4), 871.

30 R. Yuan, Y. Yang, Z. Yao and K. Zhang, High–Performance Bio–Benzoxazine Resins Derived From Natural Renewable Vanillin: Synthesis, Characterization, and Properties of Their Thermosets, *J. Appl. Polym. Sci.*, 2025, e56803.

31 W. Sheng, M. Zhong, H. Zhang and K. Zhang, Biobased bis-benzoxazine resins derived from sesamol and furfurylamine: Using natural renewable resources to access phosphorus-and halogen-free flame-retardant thermosets, *Polym. Degrad. Stab.*, 2025, **234**, 111255.

32 L. R. Kotzebue, J. s. R. de Oliveira, J. B. da Silva, S. E. Mazzetto, H. Ishida and D. Lomonaco, Development of fully biobased high-performance bis-benzoxazine under environmentally friendly conditions, *ACS Sustainable Chem. Eng.*, 2018, **6**(4), 5485–5494.

33 Y. Cao, C. Chen, X. Lu, D. Xu, J. Huang and Z. Xin, Bio-based polybenzoxazine superhydrophobic coating with active corrosion resistance for carbon steel protection, *Surf. Coat. Technol.*, 2021, **405**, 126569.

34 Y. Ohsedo and A. Kaneizumi, The Preparation of Electrolyte Hydrogels with the Water Solubilization of Polybenzoxazine, *Gels*, 2023, **9**(10), 819.

35 T. Liu, C. Hao, S. Zhang, X. Yang, L. Wang, J. Han, Y. Li, J. Xin and J. Zhang, A self-healable high glass transition temperature bioepoxy material based on vitrimer chemistry, *Macromolecules*, 2018, **51**(15), 5577–5585.

36 Z. Feng, J. Hu, H. Zuo, N. Ning, L. Zhang, B. Yu and M. Tian, Photothermal-induced self-healable and reconfigurable shape memory bio-based elastomer with recyclable ability, *ACS Appl. Mater. Interfaces*, 2018, **11**(1), 1469–1479.

37 G. Zhang, H. Feng, K. Liang, Z. Wang, X. Li, X. Zhou, B. Guo and L. Zhang, Design of next-generation cross-linking structure for elastomers toward green process and a real recycling loop, *Sci. Bull.*, 2020, **65**(11), 889–898.

38 F. Ling, Z. Liu, M. Chen, H. Wang, Y. Zhu, C. Ma, J. Wu and G. Huang, Compatibility driven self-strengthening during the radical-responsive remolding process of polyisoprene vitrimers, *J. Mater. Chem. A*, 2019, **7**(44), 25324–25332.

39 Q. Zhang, Y.-X. Deng, H.-X. Luo, C.-Y. Shi, G. M. Geise, B. L. Feringa, H. Tian and D.-H. Qu, Assembling a natural small molecule into a supramolecular network with high

structural order and dynamic functions, *J. Am. Chem. Soc.*, 2019, **141**(32), 12804–12814.

40 P. Taynton, K. Yu, R. K. Shoemaker, Y. Jin, H. J. Qi and W. Zhang, Heat–or water–driven malleability in a highly recyclable covalent network polymer, *Adv. Mater.*, 2014, **26**(23), 3938–3942.

41 S. Wang, S. Ma, Q. Li, X. Xu, B. Wang, W. Yuan, S. Zhou, S. You and J. Zhu, Facile in situ preparation of high-performance epoxy vitrimer from renewable resources and its application in nondestructive recyclable carbon fiber composite, *Green Chem.*, 2019, **21**(6), 1484–1497.

42 Y. Chen, Z. Tang, X. Zhang, Y. Liu, S. Wu and B. Guo, Covalently cross-linked elastomers with self-healing and malleable abilities enabled by boronic ester bonds, *ACS Appl. Mater. Interfaces*, 2018, **10**(28), 24224–24231.

43 Z. Wang, H. Liang, H. Yang, L. Xiong, J. Zhou, S. Huang, C. Zhao, J. Zhong and X. Fan, UV-curable self-healing polyurethane coating based on thiol-ene and Diels-Alder double click reactions, *Prog. Org. Coat.*, 2019, **137**, 105282.

44 A. Adjaoud, L. Puchot and P. Verge, High-T g and degradable isosorbide-based polybenzoxazine vitrimer, *ACS Sustainable Chem. Eng.*, 2021, **10**(1), 594–602.

45 X. Zhou, M. Shen, F. Fu, Q. Li, H. Liu and Z. Song, High strength, self-healing and hydrophobic fully bio-based polybenzoxazine reinforced pine oleoresin-based vitrimer and its application in carbon fiber reinforced polymers, *Chem. Eng. J.*, 2024, **484**, 149585.

46 Y. Qu, X. Lu and Z. Xin, Biobased polybenzoxazine vitrimer with imine bonds: shape memory, reprocessing, and degradation, *ACS Sustainable Chem. Eng.*, 2024, **12**(20), 7739–7747.

47 P. Gupta, S. K. Rastogi, B. Bhatia, S. Yadav and B. Lochab, Degradable Spiroacetal-Bridged Bioderived Polybenzoxazine Thermosets, *ACS Sustainable Chem. Eng.*, 2025, **13**(10), 4055–4067.

48 X. Xu, S. Ma, S. Wang, J. Wu, Q. Li, N. Lu, Y. Liu, J. Yang, J. Feng and J. Zhu, Dihydrazone-based dynamic covalent epoxy networks with high creep resistance, controlled degradability, and intrinsic antibacterial properties from bioresources, *J. Mater. Chem. A*, 2020, **8**(22), 11261–11274.

49 T. Kläusli, AVA Biochem: commercialising renewable platform chemical 5-HMF, *Green Process. Synth.*, 2014, **3**(3), 235–236.

50 S. P. Teong, G. Yi and Y. Zhang, Hydroxymethylfurfural production from bioresources: past, present and future, *Green Chem.*, 2014, **16**(4), 2015–2026.

51 R. Yang, R. Yang, S. Yang and K. Zhang, Hydrogen Bonding-Rich Bio-Benzoxazine Resin Provides High-Performance Thermosets and Ultrahigh-Performance Composites, *ACS Sustainable Chem. Eng.*, 2024, **12**(4), 1728–1739.

52 X. Wang, H. Niu, J. Huang, L. Song and Y. Hu, A desoxyanisoin-and furfurylamine-derived high-performance benzoxazine thermoset with high glass transition temperature and excellent anti-flammability, *Polym. Degrad. Stab.*, 2021, **189**, 109604.

53 M. Zhen, C. Wang, Y. Zhang, H. An, J. Xiao, S. Wang and Y. Liu, Ring–Opening Oligomerization Mechanism of a Vanillin–Furfurylamine–Based Benzoxazine and a Mono–Azomethine Derivative, *Macromol. Rapid Commun.*, 2023, **44**(7), 2200895.

54 S. Huang, C. Zhou and Z. Xin, Preparation and biological characteristics of LDPE/vanillin-containing benzoxazines composites for antibacterial stent materials, *Ind. Eng. Chem. Res.*, 2024, **63**(3), 1396–1408.

55 L. Han, D. Iguchi, P. Gil, T. R. Heyl, V. M. Sedwick, C. R. Arza, S. Ohashi, D. J. Lacks and H. Ishida, Oxazine ring-related vibrational modes of benzoxazine monomers using fully aromatically substituted, deuterated, 15N isotope exchanged, and oxazine-ring-substituted compounds and theoretical calculations, *J. Phys. Chem. A*, 2017, **121**(33), 6269–6282.

56 V. Duhan, S. Yadav, C. Len and B. Lochab, The mechanochemical synthesis of environmentally benign fully bio-based 4 th generation benzoxazines and their polymers: mechanistic insights into the catalytic activity of latent catalysts, *Green Chem.*, 2024, **26**(1), 483–497.

57 K. Zhang, M. Han, Y. Liu and P. Froimowicz, Design and synthesis of bio-based high-performance trioxazine benzoxazine resin via natural renewable resources, *ACS Sustainable Chem. Eng.*, 2019, **7**(10), 9399–9407.

58 J. Wang, Q. Liu, J. Yu, R. Xu, C. Wang and J. Xiong, Synthesis and characterization of benzoxazine resin based on furfurylamine, *Materials*, 2022, **15**(23), 8364.

59 S. Zhang, Q. Ran and Y. Gu, Polymerization mechanism of 1, 3-benzoxazine catalyzed by PCl5 and rearrangement of chemical structures, *Eur. Polym. J.*, 2021, **142**, 110133.

60 S. Zhang, Q. Ran, Q. Fu and Y. Gu, Preparation of transparent and flexible shape memory polybenzoxazine film through chemical structure manipulation and hydrogen bonding control, *Macromolecules*, 2018, **51**(17), 6561–6570.

61 J.-N. Wu, L. Chen, T. Fu, H.-B. Zhao, D.-M. Guo, X.-L. Wang and Y.-Z. Wang, New application for aromatic Schiff base: High efficient flame-retardant and anti-dripping action for polyesters, *Chem. Eng. J.*, 2018, **336**, 622–632.

62 X. L. Wang, R. Rathore, P. Songtipya, M. D. Jimenez-Gasco, E. Manias and C. A. Wilkie, EVA-layered double hydroxide (nano)composites: Mechanism of fire retardancy, *Polym. Degrad. Stab.*, 2011, **96**(3), 301–313.

63 X. Xu, S. Ma, J. Wu, J. Yang, B. Wang, S. Wang, Q. Li, J. Feng, S. You and J. Zhu, High-performance, command-degradable, antibacterial Schiff base epoxy thermosets: synthesis and properties, *J. Mater. Chem. A*, 2019, **7**(25), 15420–15431.

64 B. Wang, S. Ma, Q. Li, H. Zhang, J. Liu, R. Wang, Z. Chen, X. Xu, S. Wang and N. Lu, Facile synthesis of "digestible", rigid-and-flexible, bio-based building block for high-performance degradable thermosetting plastics, *Green Chem.*, 2020, **22**(4), 1275–1290.

65 X. W. Xu, S. Q. Ma, J. H. Wu, J. T. Yang, B. B. Wang, S. Wang, Q. Li, J. Feng, S. S. You and J. Zhu, High-performance, command-degradable, antibacterial Schiff base epoxy thermosets: synthesis and properties, *J. Mater. Chem. A*, 2019, 7(25), 15420–15431, DOI: **10.1039/c9ta05293c**.

66 W. Q. Xie, S. W. Huang, S. M. Liu and J. Q. Zhao, Imine-functionalized biomass-derived dynamic covalent thermosets enabled by heat-induced self-crosslinking and reversible structures, *Chem. Eng. J.*, 2021, **404**, 126598, DOI: **10.1016/j.cej.2020.126598**.